

## Supporting Information for “Does Southern Ocean surface forcing shape the global ocean overturning circulation?”

Shantong Sun,<sup>1</sup> Ian Eisenman,<sup>1</sup> and Andrew L. Stewart<sup>2</sup>

<sup>1</sup>Scripps Institution of Oceanography, University of California, San Diego, La Jolla, USA

<sup>2</sup>Department of Atmospheric and Oceanic Sciences, University of California, Los Angeles, USA

### Contents of this file

1. Text S1 to S3
2. Figures S1 to S13

### Introduction

This Supporting Information comprises three sections of text and fourteen figures. In Text S1, the CESM simulation set-up is described in detail. In Text S2, we evaluate the changes in isopycnal slope. In Text S3, we present further discussions on the diapycnal mixing in our model.

### Text S1. CESM setup

The ocean component of CESM is the Parallel Ocean Program version 2 (POP2), of which the horizontal resolution is nominally  $1^\circ$  with the north pole of the ocean grid displaced to Greenland. It has 60 vertical levels with thicknesses that range from 10 m at the sea surface to 250 m at the ocean bottom. The coupled CCSM4 simulations of the PI simulations [Gent *et al.*, 2011] and the coupled LGM simulations [Brady *et al.*, 2013], from which the forcing in this study is derived, share the same ocean grid configuration. The coupled simulations have a resolution of  $1.9^\circ \times 2.5^\circ$  for the land and atmosphere, and it has the same resolution for sea ice component as for the ocean. The unresolved mesoscale eddies are parameterized using the Gent-McWilliams scheme [Gent and McWilliams, 1990] with a thickness diffusivity that varies proportionally to the local density stratification [Gent and Danabasoglu, 2011]. The vertical convection is handled by the non-local K-Profile Parameterization (KPP) scheme [Large *et al.*, 1994].

For atmospheric forcing, including precipitation, solar radiation, surface winds speed, atmospheric pressure, and atmospheric humidity, we use output that is reported by the CCSM4 coupler every 3 hours. The atmosphere-ocean fluxes, including evaporation, wind stress, upward longwave radiation, latent heat flux, and sensible heat flux, are calculated in the ocean-only runs based on the simulated ocean state and the specified atmospheric state. For ice-related forcing, including sea ice concentration and heat flux between the ice and ocean, we use daily-mean data reported by the CCSM sea ice component (CICE). For other ice-related forcing, river runoff, and glacial runoff, we use monthly-mean data. In each case, the coupled model output is used to construct surface forcing fields that repeat every 30 years. The first 10 years of the last 30-year forcing cycle in each run are excluded in our analysis in order to avoid the adjustment associated with the jump in the forcing at the beginning of each 30-year cycle. For further details, the readers are referred to the supporting information in Sun *et al.* [2016].

---

Corresponding author: Shantong Sun, shantong@ucsd.edu

The time- and zonal-mean wind stress and wind stress curl is presented in Figure S1. Consistent with our model setup, the wind stress forcing in the Test run closely follows the LGM run in the Southern Ocean until 40°S. Unlike the wind stress forcing, surface buoyancy flux in the Test run appears to differ from LGM (Figure S2). This is because more frazil ice is formed in the LGM run due to a colder global ocean temperature, which releases more brine and increases the negative buoyancy loss close to the Antarctica. The frazil ice is formed as part of the ocean model when the temperature of seawater falls below the freezing point.

In Figure S2d, we present the zonal-mean buoyancy flux from the Southern Ocean State Estimate [SOSE; Mazloff *et al.*, 2010], which broadly resembles our PI simulation. However, the latitude where surface buoyancy forcing changes sign in SOSE is further south by 5° latitude compared to our PI simulations. Therefore, this study does not aim to reproduce the ocean circulation in the PI and LGM climate. Instead, we focus on the response of the AMOC depth to changes in the surface buoyancy forcing in the Southern Ocean.

Previous studies suggest that the simulated AMOC could be biased from the equilibrium state due to a lack of equilibration for the deep ocean circulation in climate models [e.g., Zhang *et al.*, 2013; Marzocchi and Jansen, 2017]. In order to evaluate the potential influence of model equilibrium on our results, here we use the residual-mean overturning circulation ( $\tilde{\psi}$ ), which is reported by the model and represents the sum of the Eulerian-mean overturning circulation and eddy bolus contributions, instead of the isopycnal overturning circulation ( $\psi$ ) as in the main article. The residual-mean overturning circulation is a good approximation to the isopycnal overturning circulation in the basin, where the eddy activities are relatively low. We define the AMOC strength as the maximum residual-mean overturning circulation streamfunction below 500m and the AMOC depth as the depth where  $\tilde{\psi}(y, z) = 0$  in the Atlantic averaged between 30°S and 0° (Figure S3). Note that the AMOC depth defined using  $\tilde{\psi}$  is not qualitatively different from that using  $\hat{\psi}$  (compare Figure S3 with Figure 1). Over the last 120 years, the trends in the annual-mean AMOC strength (thin lines in Figure S3) are -0.28 Sv/century, -0.17 Sv/century, and -0.64 Sv/century for the PI, Test, and LGM runs; and the trends in the annual-mean AMOC depth (thin lines in Figure S3) defined using  $\tilde{\psi}$  is -0.45 m/year, -0.04 m/year, and -0.24 m/year for the PI, Test, and LGM runs, respectively. This implies that, if these trends persist, the AMOC depth in the Test run would be closer to the PI run and farther from the LGM run following a longer model simulation. Therefore, the lack of equilibrium will not affect our conclusion that the Southern Ocean surface buoyancy forcing alone can not determine the depth of the AMOC in our model.

## Text S2. Isopycnal slope

It is hypothesized that the isopycnal slope is constant between the PI and LGM climate in Ferrari *et al.* [2014]. However, small changes in the isopycnal slope in response to surface forcing perturbations are present in both observations [Böning *et al.*, 2008] and models [e.g., Viebahn and Eden, 2010; Gent and Danabasoglu, 2011; Wolfe and Cessi, 2010] that could potentially cause discernible changes in the MOC depth. Here, we quantify the changes in the isopycnal slope between the three ocean-only simulations. Instead of calculating the isopycnal slope directly, we calculate the depth changes of isopycnals from 60°S to 30°S ( $\Delta\hat{z}_1$ ; Figure S8):

$$\Delta\hat{z} = \hat{z}(60^\circ\text{S}, \sigma_2) - \hat{z}(30^\circ\text{S}, \sigma_2). \quad (\text{S1})$$

They are mapped to depth coordinates using the mean depth of isopycnals at 50°S in Figure S8. Comparison of  $\Delta\hat{z}$  between the simulations in Figure S8b reveals that a depth difference of around 50m in the MOC depth between Test and LGM simulations could be purely attributed to the small changes in the isopycnal slope (Figure 2d), although these changes in isopycnal slope are difficult to discern by eyes (Figure S7).

### Test S3. Diapycnal mixing

Following the framework of *Walin* [1982], we can calculate the water mass transformation due to surface buoyancy forcing as

$$\mathcal{T}(\sigma_2) = -\frac{1}{T} \frac{\partial}{\partial \sigma_2} \int_0^T \iint_{90^\circ\text{S} < y < 30^\circ\text{S}} \mathcal{H}(\sigma'_2(x, y, 0, t) - \sigma_2) F_s(x, y, t) dAdt, \quad (\text{S2})$$

where  $F_s(x, y, t)$  represents the surface buoyancy flux in the Southern Ocean. If the circulation is purely adiabatic,  $\mathcal{T}(\sigma_2)$  (blue lines in Figure S9) should be the same as  $\psi(30^\circ\text{S}, \sigma_2)$  (black lines in Figure S9). The difference between the two,  $\mathcal{T}(\sigma_2) - \psi(30^\circ\text{S}, \sigma_2)$ , represents the water mass transformation due to diapycnal mixing in the Southern Ocean (red lines in Figure S9). Similar to *Newsom et al.* [2016], we find that the water mass transformation due to diapycnal mixing is substantial in the Southern Ocean in our study. By comparing Figure S9 with Figure 2 in the main article, it appears that most of the diapycnal mixing ( $\sim 15$  Sv out of 20 Sv) observed in Figure S9 occurs in the surface 1500 m in CESM.

In Figure S12, we plot the mean diapycnal diffusivity between  $60^\circ\text{S}$  and  $30^\circ\text{S}$  with respect to depth (Figure S12a) and height above the ocean bottom (Figure S12b), which is within the observed range of diapycnal diffusivity [*Waterhouse et al.*, 2014, their Fig.7]. We also calculate the mean diapycnal diffusivity close to the domain of the diapycnal and isopycnal mixing experiment in the Southern Ocean (DIMES), denoted by the two rectangles in Figure S12b. We find a diapycnal diffusivity of  $\sim 1.4 \times 10^{-4} \text{m}^2/\text{s}$  at 1500m depth, which is consistent with *Watson et al.* [2013] that concludes the diapycnal diffusivity to be  $O(10^{-4}) \text{m}^2/\text{s}$  at the same depth around the same region from tracer distributions in the DIMES project. This suggests that similar effects of diapycnal mixing on the MOC depth, as discussed in the main article, could be plausibly expected in the real ocean.

Unless in regions of deep convection or in the boundary layer, the diapycnal diffusivity profile is dominated by the parameterized tidally-driven mixing, which scales inversely with the density stratification [*Jayne*, 2009]. The diapycnal diffusivity is largest between 1.5km and 3.5km depth in Figure S12a due to its weak stratification [*Sun et al.*, 2016]. This explains the largest contribution of diapycnal mixing to the MOC depth in Figure S11b. The magnitude of the diapycnal diffusivity in the Test run falls between those of the PI run and LGM run, consistent with the diapycnal mixing in Figure S11b. This suggests that the differences in diapycnal mixing can be partly attributed to the intensity of the surface buoyancy forcing in the Southern Ocean [cf. *Sun et al.*, 2016].

Previous studies have suggested that numerical discretization of the nonlinear advection terms in tracer equation can cause substantial numerical diapycnal diffusion [e.g., *Griffies et al.*, 2000; *Hill et al.*, 2012]. Here, we quantify how much of the diapycnal mixing could be associated with discretization errors by defining an effective diapycnal diffusivity. The effective diapycnal diffusivity ( $\kappa_{\text{eff}}$ ) is defined as:

$$\hat{\omega} \frac{\partial \hat{\sigma}_2}{\partial z} = \frac{\partial}{\partial z} \left( \hat{\kappa}_{\text{eff}} \frac{\partial \hat{\sigma}_2}{\partial z} \right), \quad (\text{S3})$$

following the notation of *Munk* [1966], where the hat “ $\hat{\cdot}$ ” denotes quantities in depth coordinates as in the main article and  $\hat{\omega}$  represents the diapycnal velocity and  $\hat{\omega}(y, \hat{z}(y, \sigma_2)) = \omega(y, \sigma_2) = \frac{1}{L_x} \frac{\partial \psi(y, \sigma_2)}{\partial y}$ . A small isopycnal slope has been assumed to derive (S3). For regions below the surface mixed layer and away from deep convection zones, the water column is stably stratified and the effective diapycnal diffusivity can be obtained in  $\sigma_2$  coordinates as:

$$\kappa_{\text{eff}}(\sigma_2) = \frac{1}{L} \int_0^L \frac{\partial \hat{z}(y, \sigma_2)}{\partial \sigma_2} \left( \int_{\sigma_2^{\text{max}}}^{\sigma_2} \omega(y, \sigma'_2) d\sigma'_2 \right) dy, \quad (\text{S4})$$

where  $\kappa_{\text{eff}}(\sigma_2) = \frac{1}{L} \int_0^L \hat{\kappa}_{\text{eff}}(y, \hat{z}(y, \sigma_2)) dy$ ,  $L$  is the meridional length of the integration, is the diapycnal velocity in  $\sigma_2$  coordinates, and  $\hat{z}(y, \sigma_2)$  represents the mean depth of isopycnal, as defined in the main article.

For comparison, the parameterized diapycnal diffusivity is also mapped to  $\sigma_2$  coordinates as

$$\kappa(\sigma_2) = \frac{1}{T} \int_0^T \frac{1}{A} \iint \kappa_m(x, y, z, t)|_{\sigma'_2(x, y, z, t)=\sigma_2} dx dy dt, \quad (\text{S5})$$

where  $\kappa_m(x, y, z, t)$  is the model reported diapycnal diffusivity, and  $A$  represents the integral area on isopycnals.

We compare the diagnosed effective diapycnal diffusivity  $\kappa_{\text{eff}}$  with the model reported diapycnal diffusivity  $\kappa$  in Figure S13. It appears that the effective diapycnal diffusivity is approximately the same as the the model-reported value, implying that the numerical diapycnal mixing is not playing a significant role in CESM. Here, we have limited the calculation of  $\kappa_{\text{eff}}$  and  $\kappa$  in the deep ocean and within 30°S and 30°N. This is because a stable stratification is required in Equations (S3) and (S5) and the calculation might be not reliable in the Southern Ocean. Therefore, we cannot exclude the possibility of a larger fraction of the diapycnal mixing being due to numerical discretization errors in the Southern Ocean.

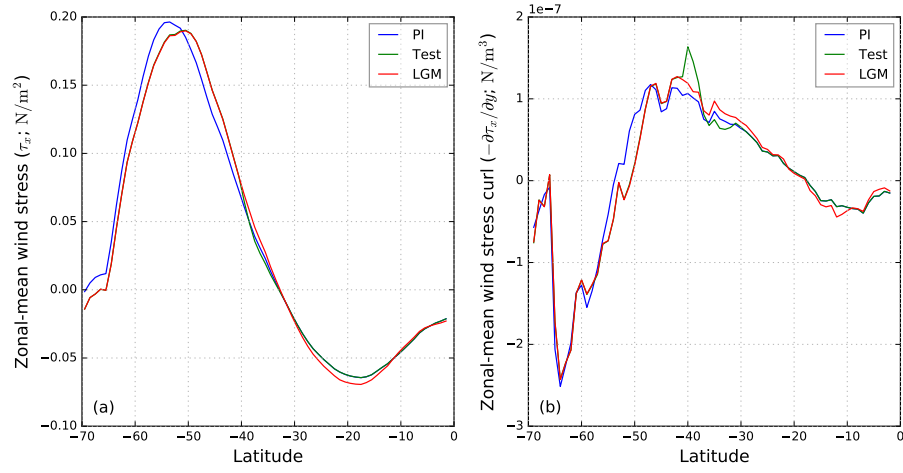


**Figure S1.** Zonal mean wind stress (a) and wind stress curl (b). Note that the slightly enhanced wind stress curl in the Test simulation close to 40°S is due to the feathering of the forcing fields between 40°S and 30°S.

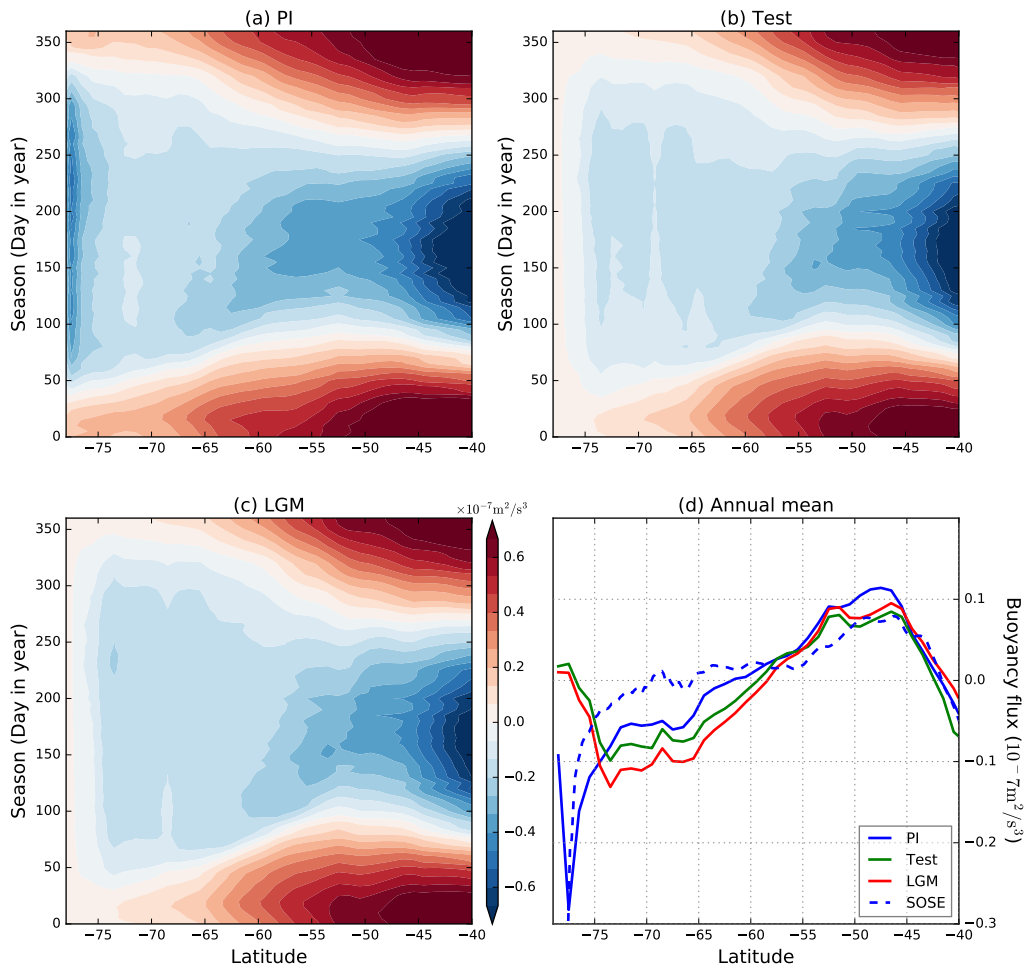


**Figure S2.** Long-term mean seasonally-varying zonal-mean buoyancy flux (a-c) and annual-mean buoyancy flux (d) from the three ocean-only simulations. The time- and zonal-mean buoyancy flux over years 2005-2010 from the Southern Ocean State Estimate [SOSE; Mazloff *et al.*, 2010] is plotted in panel d as a blue dashed line for comparison.

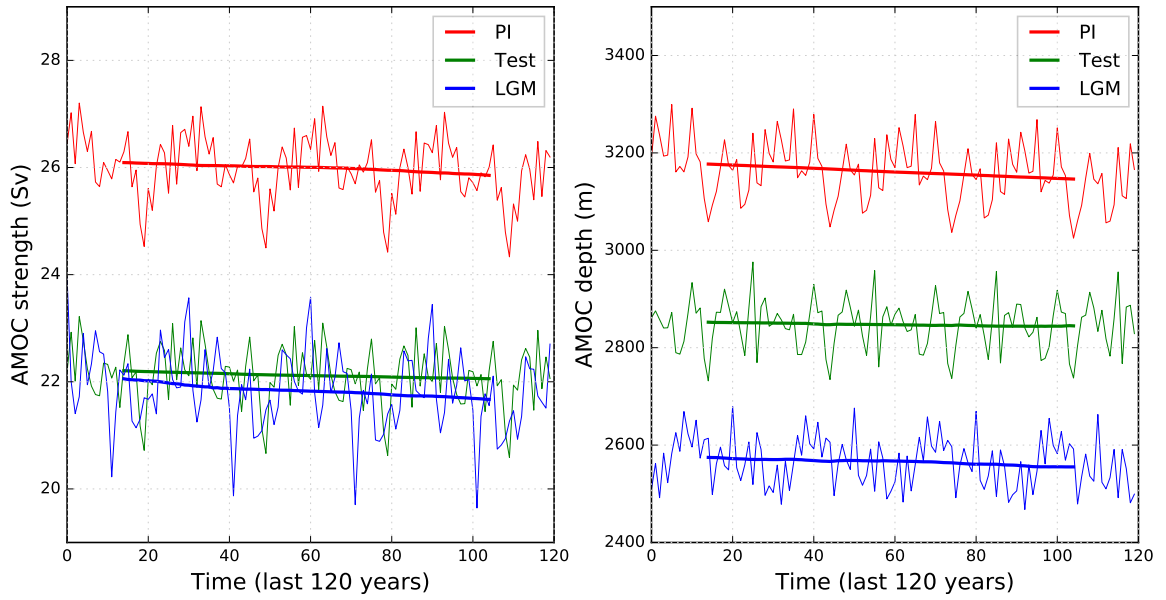


**Figure S3.** Annual-mean AMOC strength (left) and depth (right) over the last 120 years of the simulations. The thick lines represent 30-year running averages of the annual-mean data. The AMOC depth is averaged between 30°S and 0° in the Atlantic Ocean.

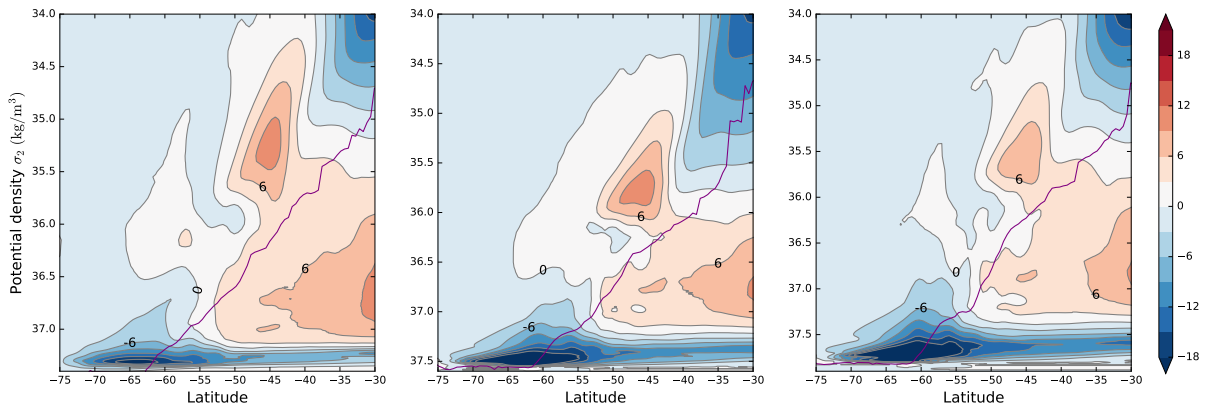


**Figure S4.** The MOC streamfunction on  $\sigma_2$  coordinates in the Southern Ocean, with the contours and colorbar labeled in units of Sv. The purple line represents the maximum potential density that appears in the surface mixed layer at each latitude for any time and any longitude. Therefore, isopycnals below the purple line always lie below the surface mixed layer.

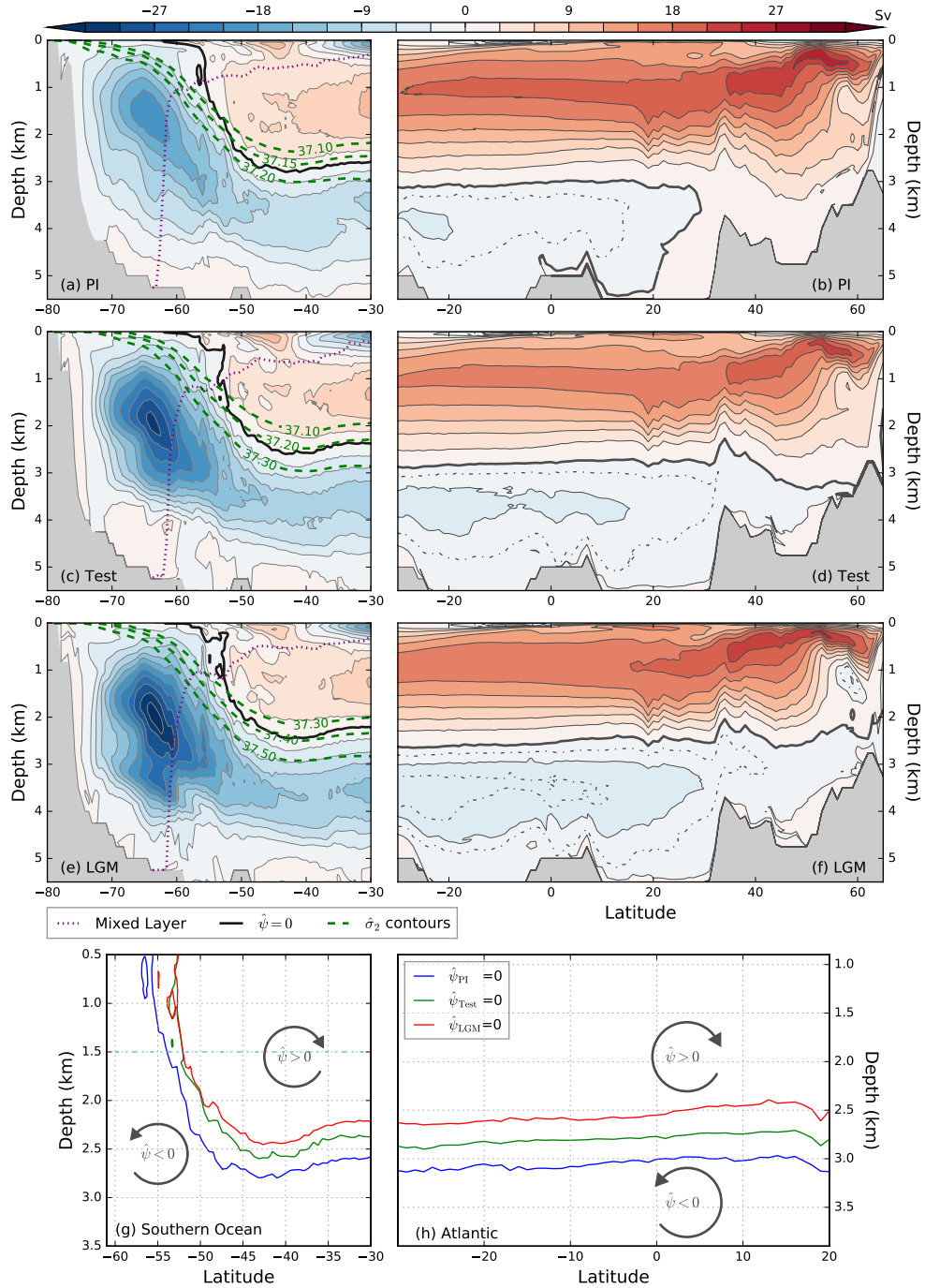


**Figure S5.** As in Figure 1 of the main text, but using un-smoothed data in the Southern Ocean.



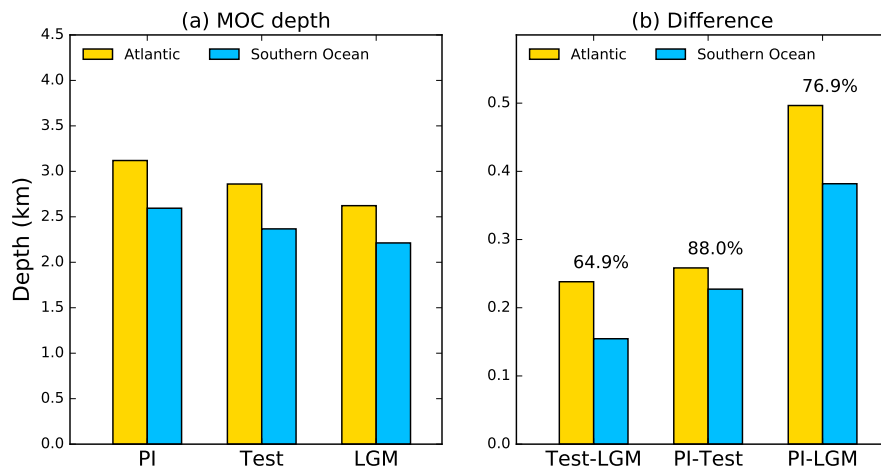


**Figure S6.** (a) MOC depth in Atlantic and in the Southern Ocean at 30°S and (b) comparison of the MOC depth between the three simulations. The percentage in panel (b) shows the ratio between the MOC depth differences in the Southern Ocean vs that in the Atlantic Ocean. This implies that the AMOC depth changes can be mostly attributed to the MOC changes in the Southern Ocean in our simulations. The lower percentage for “Test-LGM” and “PI-LGM” in (b) implies the importance of the North Atlantic processes in modifying the inter-basin transport of NADW between the Atlantic ocean and the Pacific ocean, which will be discussed in a later study.

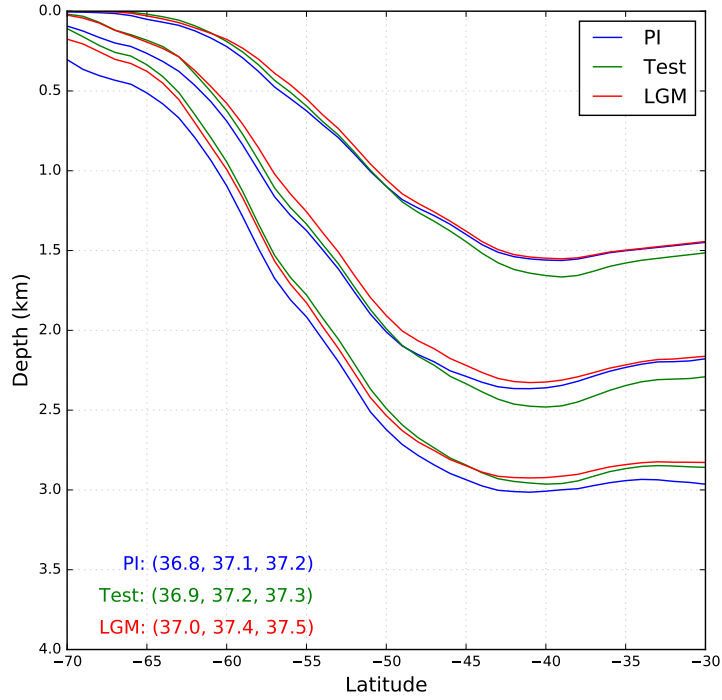


**Figure S7.** Contours of  $\hat{\sigma}_2(y, z)$  to compare the isopycnal slopes between the three simulations. The potential densities for the three plotted isopycnals (from top to bottom) in each simulation are provided in the bottom left in units of  $\text{kg/m}^3$ .

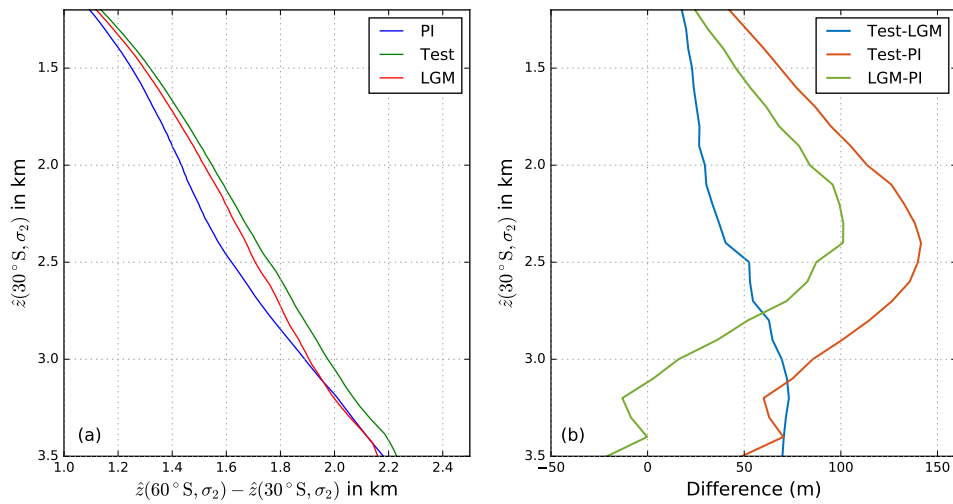


**Figure S8.** (a) Depth change of isopycnals  $\Delta\hat{z}$  from  $60^\circ\text{S}$  to  $30^\circ\text{S}$ . (b) Difference in  $\Delta\hat{z}$  between the three simulations.

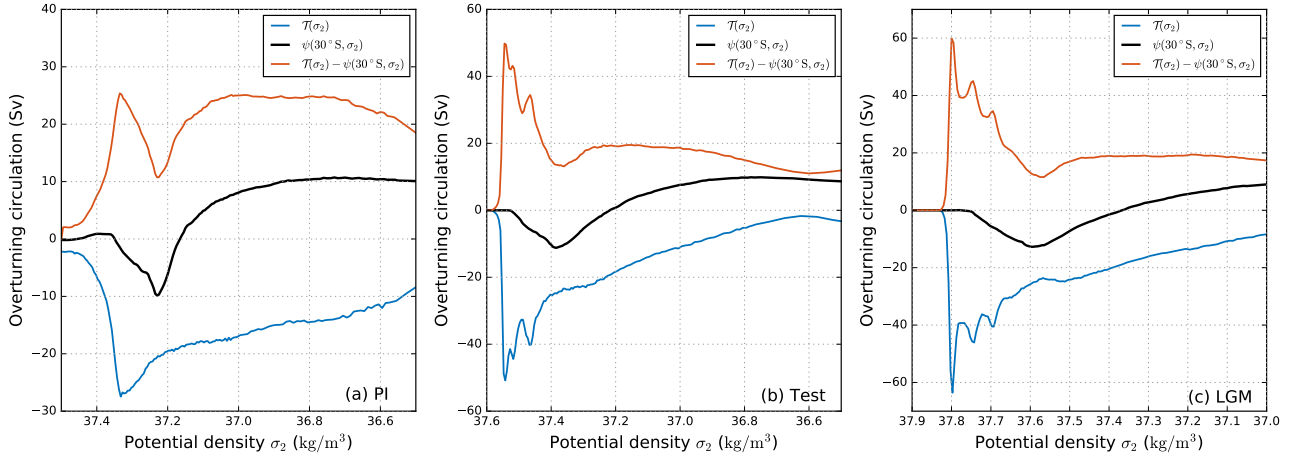


**Figure S9.** Water mass transformation due to surface buoyancy flux (blue lines), overturning circulation at 30°S (black lines), and the residual that is due to diapycnal transport (red lines). This is not sensitive to the reference pressure, i.e., the strong diapycnal transformation is similar if calculated using  $\sigma_0$  or  $\sigma_4$  coordinates.

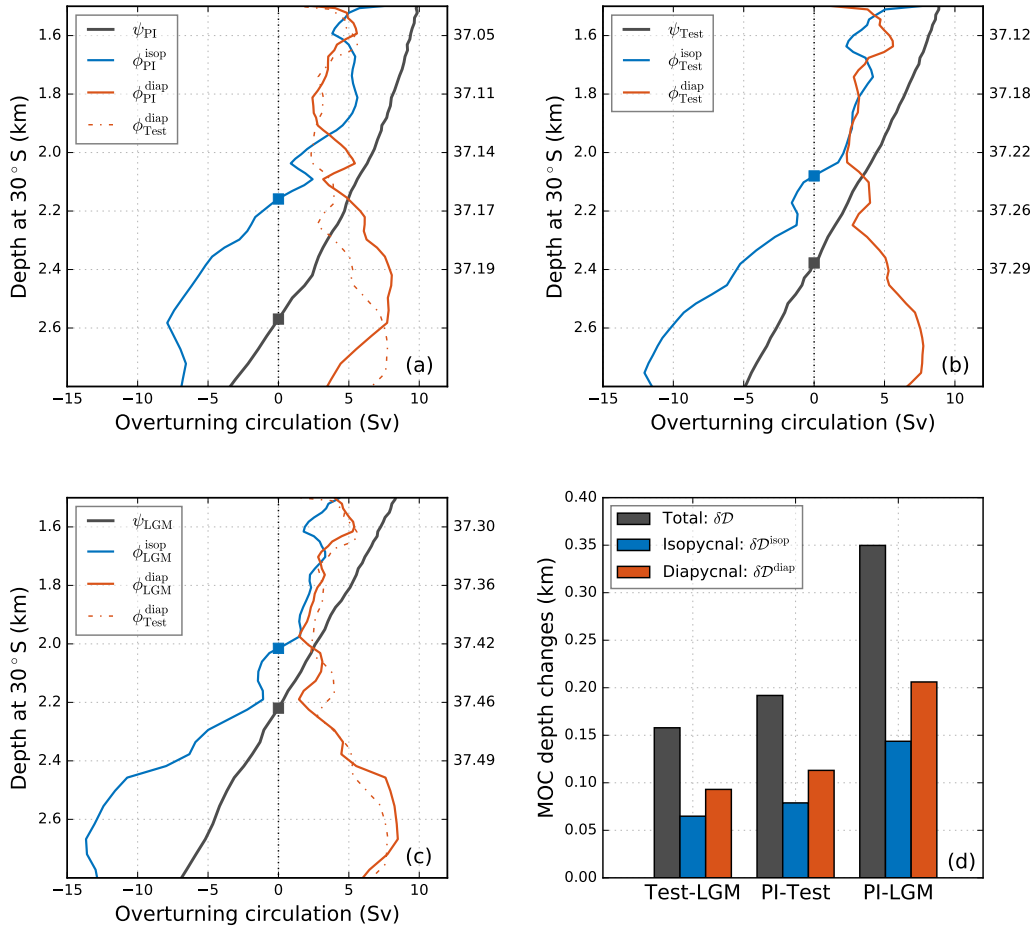


**Figure S10.** As in Figure 2 of the main text, but using un-smoothed data in the Southern Ocean.

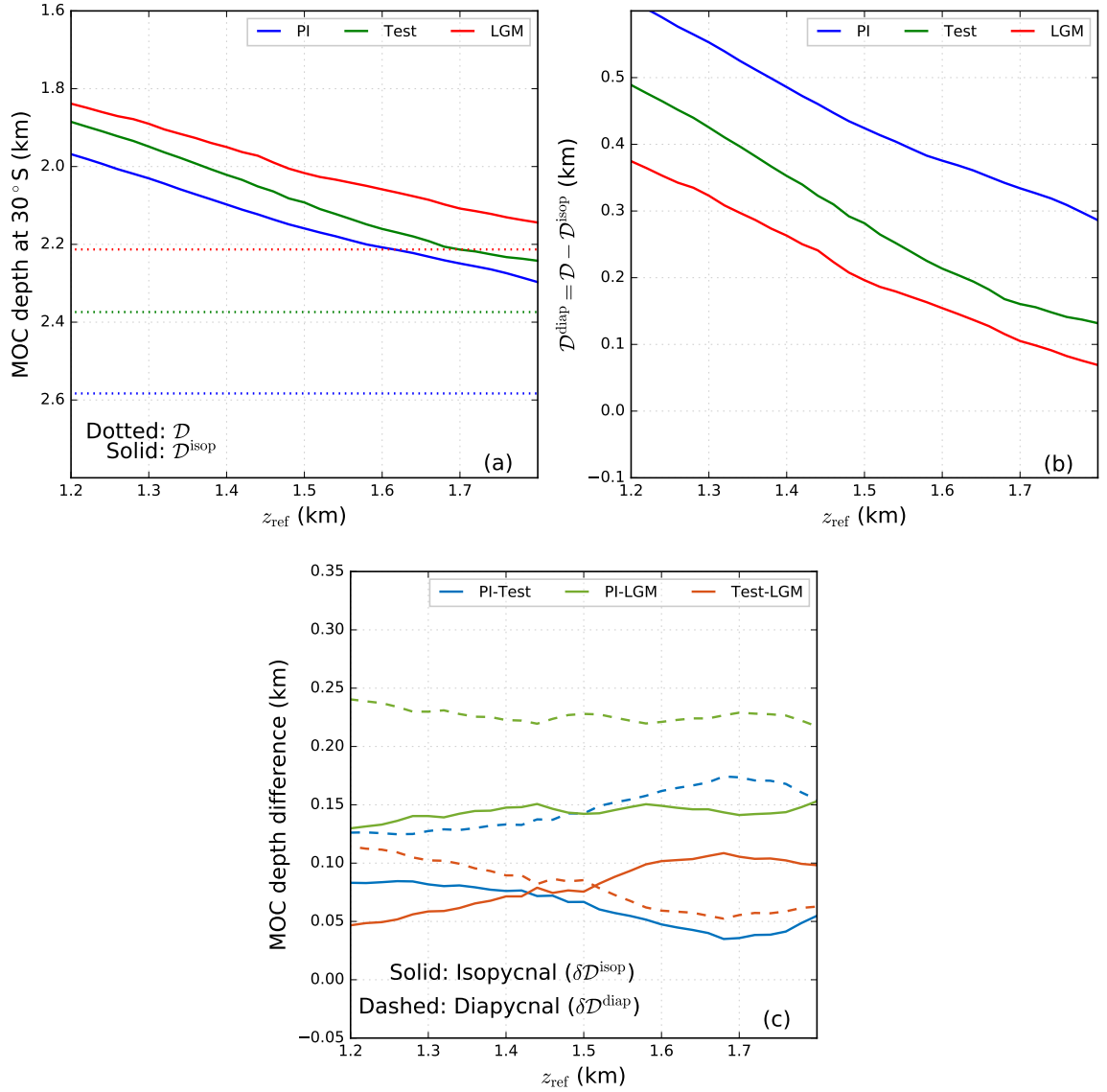


**Figure S11.** Dependence of  $\mathcal{D}$  (a),  $\mathcal{D}^{\text{isop}}$  (a),  $\mathcal{D}^{\text{diap}}$  (b),  $\delta\mathcal{D}^{\text{isop}}$ , and  $\delta\mathcal{D}^{\text{diap}}$  on the reference depth  $z_{\text{ref}}$  as discussed in Section 4. The y-axis is reversed in (a) to show that higher  $\mathcal{D}$  means deeper depth. The contribution of diapycnal mixing to the MOC depth ( $\mathcal{D}^{\text{diap}}$ ) decreases with the reference depth because the integral area (represented by  $L_y$  in Figure 3) is smaller for larger  $z_{\text{ref}}$ . However, the contribution of diapycnal mixing to the MOC depth difference is insensitive to the reference depth.

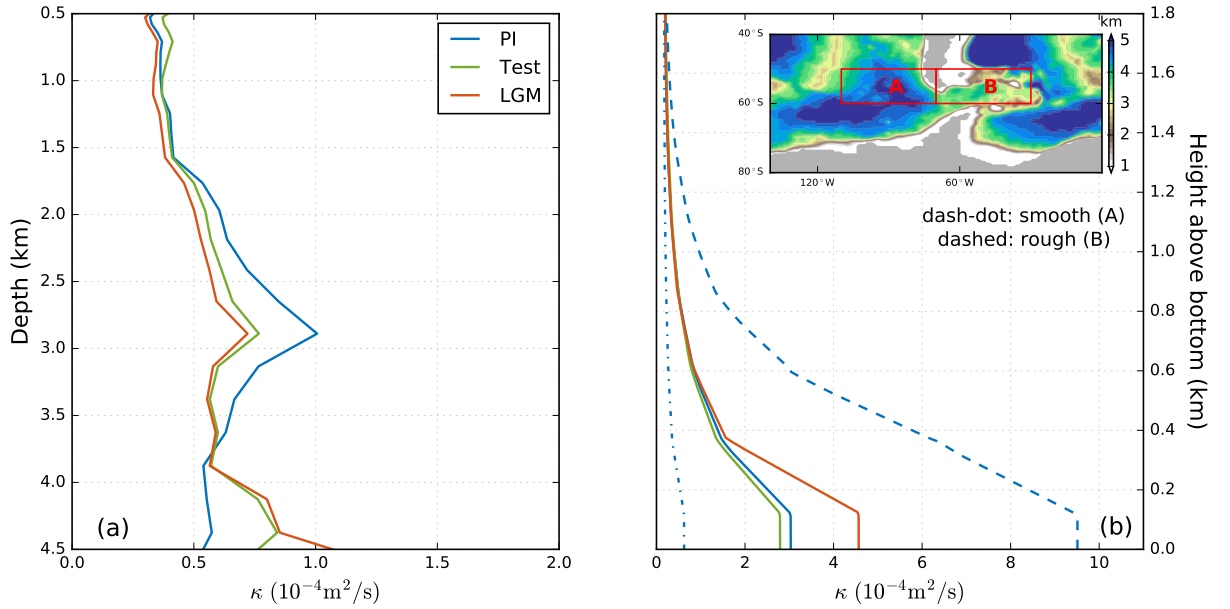


**Figure S12.** Diapycnal diffusivity averaged on constant depth (a) and on constant height above bottom topography (b) between  $60^\circ\text{S}$  and  $30^\circ\text{S}$ . Deep convection regions ( $\kappa \approx 1 \text{m}^2/\text{s}$ ) are excluded. In Panel (b), only regions deeper than 2000m are considered following *Waterhouse et al.* [2014]. This explains why diapycnal diffusivity is the largest in the PI run in Panel (a) between 1.5km and 3.5 km depth, due to its weak stratification, but it is not seen in Panel (b). The subplot within Panel (b) shows the bathymetry (km) close to the Drake passage. To compare with observations, we calculate the mean diapycnal diffusivity profiles over smooth topography (dash-dotted lines; A) and rough topography (dashed lines; B) close to the Drake passage for the PI simulation. And we find that both diapycnal diffusivity profiles are within the observed range given by *Waterhouse et al.* [2014]. The regions denoted by “A” and “B” correspond approximately to the domain of the DIMES project, where *Mashayek et al.* [2017] concludes the diapycnal mixing to be  $O(10^{-4})\text{m}^2/\text{s}$  at 1500m depth. We averaged the diapycnal diffusivity at 1500m depth over the region denoted by “A” and “B”, and we find a diapycnal diffusivity of  $1.4 \times 10^{-4} \text{m}^2/\text{s}$ , consistent with *Watson et al.* [2013].

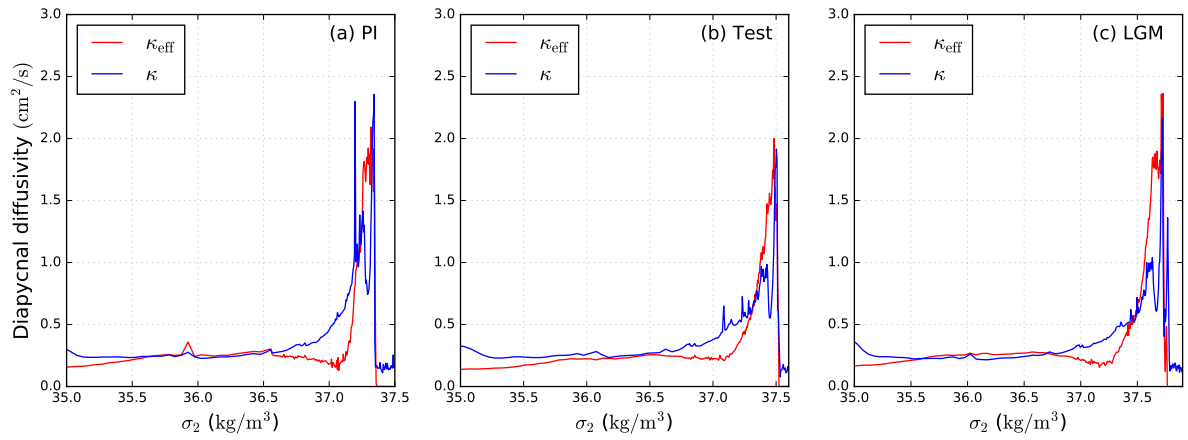


**Figure S13.** Effective diapycnal diffusivity ( $\kappa_{\text{eff}}$ , defined in Equation (S4)) and model-reported diapycnal diffusivity ( $\kappa$ , defined in Equation (S5)) calculated between  $30^\circ\text{S}$  and  $30^\circ\text{N}$ . The potential density range covers the depth range from intermediate depth to the ocean bottom.

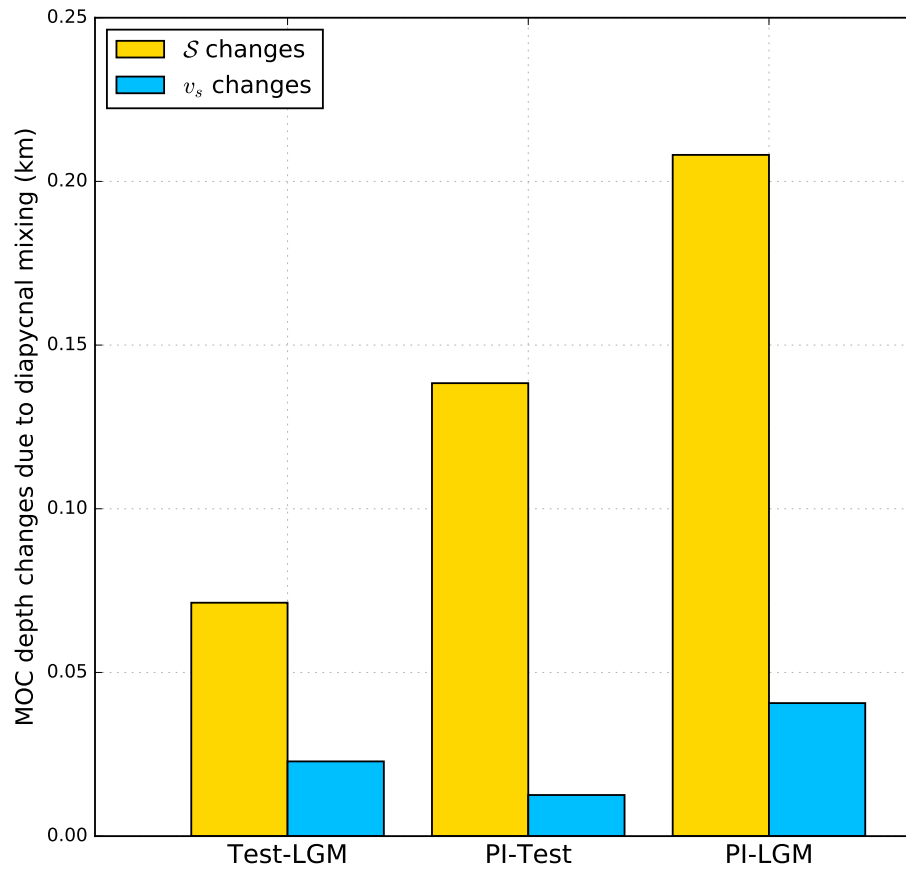


**Figure S14.** Contribution of diapycnal mixing to MOC depth changes due to changes in  $S$  and  $v_s$  according to Equation (9).

## References

- Böning, C. W., A. Dispert, M. Visbeck, S. Rintoul, and F. U. Schwarzkopf (2008), The response of the Antarctic Circumpolar Current to recent climate change, *Nat. Geosci.*, *1*(12), 864–869.
- Brady, E. C., B. L. Otto-Bliesner, J. E. Kay, and N. Rosenbloom (2013), Sensitivity to glacial forcing in the CCSM4, *J. Clim.*, *26*(6), 1901–1925.
- Ferrari, R., M. F. Jansen, J. F. Adkins, A. Burke, A. L. Stewart, and A. F. Thompson (2014), Antarctic sea ice control on ocean circulation in present and glacial climates, *Proc. Natl. Acad. Sci.*, *111*(24), 8753–8758.
- Gent, P. R., and G. Danabasoglu (2011), Response to increasing Southern Hemisphere winds in CCSM4, *J. Clim.*, *24*(19), 4992–4998.
- Gent, P. R., and J. C. McWilliams (1990), Isopycnal mixing in ocean circulation models, *J. Phys. Oceanogr.*, *20*(1), 150–155.
- Gent, P. R., G. Danabasoglu, L. J. Donner, M. M. Holland, E. C. Hunke, S. R. Jayne, D. M. Lawrence, R. B. Neale, P. J. Rasch, M. Vertenstein, et al. (2011), The community climate system model version 4, *J. Clim.*, *24*(19), 4973–4991.
- Griffies, S. M., R. C. Pacanowski, and R. W. Hallberg (2000), Spurious diapycnal mixing associated with advection in az-coordinate ocean model, *Mon. Weather Rev.*, *128*(3), 538–564.
- Hill, C., D. Ferreira, J.-M. Campin, J. Marshall, R. Abernathey, and N. Barrier (2012), Controlling spurious diapycnal mixing in eddy-resolving height-coordinate ocean models—insights from virtual deliberate tracer release experiments, *Ocean Modell.*, *45*, 14–26.
- Jayne, S. R. (2009), The impact of abyssal mixing parameterizations in an ocean general circulation model, *J. Phys. Oceanogr.*, *39*(7), 1756–1775.
- Large, W. G., J. C. McWilliams, and S. C. Doney (1994), Oceanic vertical mixing: A review and a model with a nonlocal boundary layer parameterization, *Rev. Geophys.*, *32*(4), 363–403.
- Marzocchi, A., and M. F. Jansen (2017), Connecting Antarctic sea ice to deep-ocean circulation in modern and glacial climate simulations, *Geophys. Res. Lett.*, *44*(12), 6286–6295.
- Mashayek, A., R. Ferrari, S. Merrifield, J. R. Ledwell, L. St Laurent, and A. Naveira Garabato (2017), Topographic enhancement of vertical turbulent mixing in the Southern Ocean, *Nat. Commun.*, *8*, 14,197.
- Mazloff, M. R., P. Heimbach, and C. Wunsch (2010), An eddy-permitting Southern Ocean state estimate, *J. Phys. Oceanogr.*, *40*(5), 880–899.
- Munk, W. H. (1966), Abyssal recipes, in *Deep-Sea Res.*, vol. 13, pp. 707–730, Elsevier.
- Newsom, E. R., C. M. Bitz, F. O. Bryan, R. Abernathey, and P. R. Gent (2016), Southern Ocean deep circulation and heat uptake in a high-resolution climate model, *J. Clim.*, *29*(7), 2597–2619.
- Sun, S., I. Eisenman, and A. L. Stewart (2016), The influence of southern ocean surface buoyancy forcing on glacial-interglacial changes in the global deep ocean stratification, *Geophys. Res. Lett.*, *43*(15), 8124–8132.
- Viebahn, J., and C. Eden (2010), Towards the impact of eddies on the response of the Southern Ocean to climate change, *Ocean Modell.*, *34*(3), 150–165.
- Walín, G. (1982), On the relation between sea-surface heat flow and thermal circulation in the ocean, *Tellus*, *34*(2), 187–195.
- Waterhouse, A. F., J. A. MacKinnon, J. D. Nash, M. H. Alford, E. Kunze, H. L. Simmons, K. L. Polzin, L. C. St. Laurent, O. M. Sun, R. Pinkel, et al. (2014), Global patterns of diapycnal mixing from measurements of the turbulent dissipation rate, *J. Phys. Oceanogr.*, *44*(7), 1854–1872.
- Watson, A. J., J. R. Ledwell, M.-J. Messias, B. A. King, N. Mackay, M. P. Meredith, B. Mills, and A. C. Naveira Garabato (2013), Rapid cross-density ocean mixing at mid-



- depths in the Drake Passage measured by tracer release, *Nature*, 501(7467), 408.
- Wolfe, C. L., and P. Cessi (2010), What sets the strength of the middepth stratification and overturning circulation in eddying ocean models?, *J. Phys. Oceanogr.*, 40(7), 1520–1538.
- Zhang, X., G. Lohmann, G. Knorr, and X. Xu (2013), Different ocean states and transient characteristics in Last Glacial Maximum simulations and implications for deglaciation, *Clim. Past*, 9(5), 2319.